ELSEVIER

Journal of Fluids and Structures 24 (2008) 664–679

JOURNAL OF FLUIDS AND STRUCTURES

www.elsevier.com/locate/jfs

Free-stream turbulence effects on vortex-induced vibration of two side-by-side elastic cylinders

X.Q. Wang[a], R.M.C. So[a,*], W.-C. Xie[b], J. Zhu[b]

[a]*Department of Mechanical Engineering, The Hong Kong Polytechnic University, Hung Hom, Kowloon, HKSAR, PRC*
[b]*Department of Civil and Environmental Engineering, Faculty of Engineering, University of Waterloo, Waterloo, Ont., Canada*

Received 2 May 2007; accepted 28 October 2007
Available online 21 December 2007

Abstract

The effect of free-stream turbulence on vortex-induced vibration of two side-by-side elastic cylinders in a cross-flow was investigated experimentally. A turbulence generation grid was used to generate turbulent incoming flow with turbulence intensity around 10%. Cylinder displacements in the transverse direction at cylinder mid-span were measured in the reduced velocity range $1.45 < U_{r0} < 12.08$, corresponding to a range of Reynolds number (Re), based on the mean free-stream velocity and the diameter of the cylinder, between Re = 5000–41 000. The focus of the study is on the regime of biased gap flow, where two cylinders with pitch ratio (T/D) varying from 1.17 to 1.90 are considered. Results show that the free-stream turbulence effect is to enhance the vortex-induced force, thus to restore the large-amplitude vibration associated with the lock-in resonance. However, the enhancement is significant at a different Strouhal number (St) for different pitch ratios. When the spacing between two cylinders is relatively small ($1.17 < T/D < 1.50$), the enhancement is significant at $\mathrm{St} \approx 0.1$. When the spacing is increased, the Strouhal number at which the enhancement is significant shifts to $\mathrm{St} \approx 0.16$. This enlarges the range of reduced velocity to be concerned. An energy analysis showed that free-stream turbulence feeds energy to the cylinder at multiple frequencies of vortex shedding. Therefore, the lock-in region is still of main concern when the approach flow is turbulent.

1. Introduction

It is well known that flow-induced vibrations of bluff bodies in a cross-flow is affected by a host of excitations; chief among them are instability-induced excitation, movement-induced excitation, and extraneously-induced excitation (Naudascher and Rockwell, 1994). In the context of external flow-induced vibration and instability of bluff bodies, these excitations are associated with the vortex-induced force, the motion-dependent force, and the turbulence-induced buffeting force, respectively. The buffeting force is present as long as there is free-stream turbulence in the oncoming flow and is not dependent on the motion of the bluff bodies (So and Savkar, 1981). This effect is derived from the flow around the bluff bodies and the behavior in the wakes. For example, in the case of a flow past a single cylinder, a strong effect of free-stream turbulence is observed in the states of transition of the wake, the shear layers, and the boundary layers (Zdravkovich, 1997). Consequently, free-stream turbulence promotes critical transition at a Reynolds number (Re) lower than that for a nonturbulent uniform flow. Here, $\mathrm{Re} = U_\infty D/\nu$ is usually defined, where U_∞ is the mean

*Corresponding author.
E-mail address: mmmcso@polyu.edu.hk (R.M.C. So).

0889-9746/$ - see front matter © 2007 Elsevier Ltd. All rights reserved.
doi:10.1016/j.jfluidstructs.2007.10.007

free-stream velocity, D is the hydraulic diameter of the bluff bodies, and v is the fluid kinematic viscosity. Experimental measurements of the behavior of the mean drag coefficient $\bar{C}_D$ versus Re reveal that the Re at which the drag crisis occurs is reduced as free-stream turbulence increases (So and Savkar, 1981). Free-stream turbulence, therefore, has a significant effect on the buffeting force and hence the vibration behavior of the bluff bodies. Moreover, it has been found that free-stream turbulence enhances the vortex-induced force in the range enclosing the lock-in resonance region, and enhances the motion-dependent force in the range of relatively large reduced velocity, $U_{r0} = U_\infty/f^*_{n0}D$ (So et al., 2007), where f^*_{n0} is the dimensional natural frequency of the cylinder in still air.

In the case of two side-by-side cylinders, the situation becomes more complex due to the presence of wake interference when the cylinders are in close proximity to each other. The interference could affect vortex shedding from the two cylinders and the associated flow-induced forces. The extent of the interference effect depends on many parameters; the more important of these is the pitch ratio, T/D, where T is the separation distance measured between cylinder centers. This flow interference behavior has been investigated by numerous researchers; recent reviews have been provided by Chen (1986), Wradlaw (1994), and Zdravkovich (2003).

When the two cylinders are stationary, the interference behavior can be classified according to T/D (Zdravkovich, 2003). For a finite range of Re, two coupled vortex streets are observed in the first regime where T/D is moderate, i.e., $2.3 < T/D < 4$. The two vortex streets have the same shedding frequency but are coupled in an out-of-phase mode. In the second regime which covers the range $1.1 < T/D < 2.3$, a biased gap flow pattern appears. The third regime is characterized by two strongly coupled wakes which behave like the wake behind a single bluff body. The T/D in this regime is given by $T/D < 1.1$. This classification still holds when the two cylinders are freely vibrating due to the excitation of flow-induced forces, except that the T/D values separating these regimes are slightly modified.

Extensive studies have been carried out to investigate wake interference patterns associated with the biased gap flow, experimentally and numerically (Bearman and Wadcock, 1973; Kim and Durbin, 1988; Chang and Song, 1990; Slaouti and Stansby, 1992; Ng et al., 1997; Sumner et al., 1997, 1999; Guillaume and LaRue, 1999, 2003; Meneghini et al., 2001; Chen et al., 2003; Jester and Kallinderis, 2003). The most noteworthy feature is that the biased gap flow induces multiple frequencies of vortex shedding, giving rise to Strouhal numbers (St) around 0.1 and 0.3, associated with a wide wake behind one cylinder and a narrow wake behind the other, respectively. Here, $\mathrm{St} = f^*_s D/U_\infty$ is defined, where f^*_s is the dimensional vortex shedding frequency. The biased gap flow is usually considered to be bistable, intermittently changing from one side to the other. However, Williamson (1985) showed that there also exist three St values around 0.1, 0.2, and 0.3, respectively. In a recent study, Alam et al. (2003) showed that there exists an intermediate wake pattern, where the direction of the gap flow is parallel to that of the free stream and the corresponding value of St is around 0.2.

The Reynolds number appears to play an important role in the appearance of the biased gap flow. Through a theoretical analysis of wake behavior in the range of $\mathrm{Re} = 90$–150 and $T/D = 1.6$–3.3, Peschard and Le Gal (1996) showed that increasing Re has the same effect as increasing T/D. Xu et al. (2003) experimentally investigated the effect of Re on the dominant frequencies of the flow velocity in the range of $\mathrm{Re} = 150$–$14\,300$ and $T/D = 1.2$–1.6. For a given T/D, one single vortex street was found at low Re, which is associated with one single dominant frequency in the flow velocity. As Re increases, the wake begins to transition to a behavior characterized by two asymmetric vortex streets associated with two dominant frequencies in the flow velocity. The transition was conjectured to be due to the fact that the gap flow breaks up a small closed wake (arising from the near-wall effect) when Re exceeds a critical value, leading to two (one narrow and one wide) asymmetric vortex streets in the wake. Through numerical simulations, Wang et al. (2007) showed that there exists a critical value of Re, at which the wake transits from stable-biased gap flow to unstable gap flow, giving rise to nonstationary vortex-induced forces. For the pitch ratio $T/D = 1.7$, the critical Re is around 100.

The effects of the biased gap flow on vortex-induced forces acting on the structures and subsequent structural responses have not been fully understood. Ichioka et al. (1997) investigated the fluid–elastic vibration of two rigid circular cylinders at $\mathrm{Re} = 1000$ for $T/D = 1.5$. The two cylinders vibrate in a reverse phase mode. There is only one dominant frequency due to synchronization with the natural frequency of the cylinder. However, there is another frequency peak associated with each cylinder. Zhou et al. (2001) experimentally investigated the interference behavior of two fixed–fixed elastic cylinders in a cross-flow. Three pitch ratios, $T/D = 1.13$, 1.7, and 3.0, were studied. It is shown that cylinder vibrations are essentially out-of-phase at $T/D = 3.0$, while in-phase at $T/D = 1.13$. A significant finding is that synchronization occurs at several reduced velocities, corresponding to the first several natural frequencies of the system. So and Wang (2003) used a finite element method to simulate flow-induced vibration of two side-by-side cylinders with $T/D = 1.7$ in cross-flows at $\mathrm{Re} = 800$. The method of short-time Fourier transform was used to investigate nonstationary features of the flow-induced forces and the corresponding cylinder vibrations. It was shown that three different types of power spectrum exist, i.e.: type A, a spectrum with a single dominant frequency occurring at $\mathrm{St} = 0.2$; type B, a spectrum with two dominant frequencies occurring at $\mathrm{St} = 0.1$ and 0.2 or $\mathrm{St} = 0.2$ and 0.3; and

type C, a spectrum with three dominant frequencies occurring at St = 0.1, 0.2, and 0.3. These three types of spectrum appear intermittently in a random way.

The mechanism of the biased gap flow has not been fully understood. In the literature, a physical interpretation has been proposed by Peschard and Le Gal (1996), where the wake interference was modeled by a pair of coupled Landau equations, and the biased gap flow was shown to be one of the features of Hopf bifurcations. However, this model was only applicable to a range of low Reynolds numbers (Re < 150), hence more work covering a wider range of Re needs to be carried out to investigate the effect of Re on this biased gap flow behavior. Since free-stream turbulence has a significant effect on the wake flow in the single cylinder case, it could have an influence on the biased gap flow in the two-cylinder flow case also. An experimental study that aims to investigate the influence of free-stream turbulence on the features of cylinder vibrations and fluctuating lift force coefficients in the regime of biased gap flow could contribute to further the understanding of biased gap flow.

It is in this spirit that the present study proposes to investigate flow-induced vibration of two side-by-side elastic cylinders in a nonturbulent uniform and a turbulent approach flow. The objective of the study is to further understand the effect of wake interference on flow-induced vibrations in the regime of biased gap flow under the influence of a nonturbulent uniform or a turbulent approach flow. This is important to many branches of engineering, such as in the design of heat exchangers, nuclear reactors, offshore drilling platforms, and overhead transmission lines. Understanding of this interaction behavior in complex flow environments could help the design of these engineering systems to avoid operating too close to any resonance or instability regions.

As such, the present study is an extension of a previous study on flow-induced vibration of a single elastic cylinder in turbulent approach flow (So et al., 2007). In the experiments, the range of Re investigated varies from 5×10^3 to 4.1×10^4, and the pitch ratio increases from 1.17 to 1.90, thus straddling the biased gap flow regime. A turbulence generation grid is used to generate homogeneous, isotropic turbulence in the approach flow. The turbulence intensity as determined from the flow velocity measured using a laser Doppler anemometer (LDA) is approximately 10%. In the experiments, the two cylinders are fixed at their ends and are allowed to freely vibrate in a turbulent cross-flow. The vibration displacement at cylinder mid-span in the cross-flow direction is measured using a laser vibrometer. Comparison with previous one-cylinder experimental results is presented to demonstrate the effect of wake interference. Extensive data analysis is carried out to investigate the effect of free-stream turbulence on the amplitude of cylinder vibration and on the dominant frequencies.

2. Experimental set-up

The experimental set-up is essentially identical to that used for the study of flow-induced vibration of one single cylinder in a turbulent cross-flow (So et al., 2007). Use of this identical facility would allow the present two-cylinder data to be compared with the previously obtained one-cylinder results. A brief description of the experimental set-up is given here; the readers may refer to So et al. (2007) for further details.

2.1. Wind tunnel and turbulence generation grid

Experiments were carried out in a closed loop wind tunnel. A sketch of the experimental set-up is shown in Fig. 1(a). The wind tunnel has a 2400 mm long test section with a 600 mm × 600 mm cross section. The free-stream velocity U_∞ of the approach flow can be continuously varied from 0 to 40 m/s. In the experiment, a turbulence generation grid was installed at the exit of the contraction section to generate homogeneous, isotropic turbulence in the test section. A grid of the square mesh type (Fig. 1(b)) was adopted. The dimensions of the grid are $d_g = 20$ mm and $l_g = 50$ mm. When the turbulence generation grid is installed, the maximum possible U_∞ is reduced to 25 m/s.

The turbulence intensity of the approach flow, Tu, was determined from the measured flow velocities using an LDA. It is found that Tu is approximately 10% for the Re range studied. The distributions of the mean flow velocity and the turbulent intensity across the cross-section of the test section were checked, showing that the grid-generated turbulent flow is homogeneous over the range of Re investigated.

2.2. Cylinder model

Two identical acrylic tubes are used as the elastic cylinder model. The outer and inner diameters of the tube are $D = 30$ mm and $d = 26$ mm, respectively; thus the aspect ratio is 20, while the blockage ratio will vary with the pitch ratio, T/D. Based on $D = 30$ mm, the range of Re varies from 5000 to 41 000. The reduced velocity $U_{r0} = U_\infty / f^*_{n0} D$, based on the fundamental natural frequency of the cylinder in still air f^*_{n0}, varies from 1.45 to 12.08.

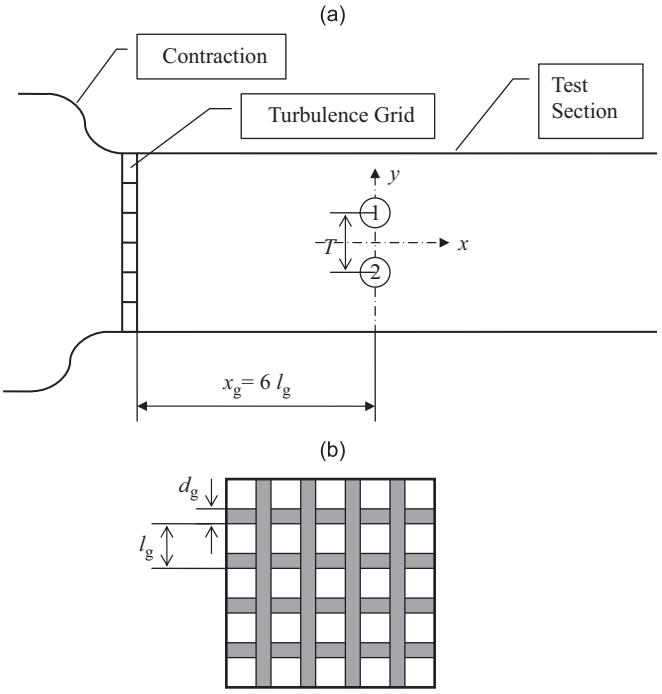

Fig. 1. Illustration of the wind tunnel with turbulence generation grid installed: (a) wind tunnel and (b) turbulence generation grid.

Table 1
Properties of the elastic cylinder model

Cylinder material	D (mm)	M (kg/m)	EI (N m^2)	M_r	f_n^* (Hz)	ζ_s
Acrylic	30	0.208	11.8	195.5	69	0.12

The cylinder model was horizontally mounted in the mid-plane of the test-section and 300 mm downstream from the exit plane of the contraction (also the turbulence generation grid when it was installed). The two cylinders were arranged side-by-side, and the pitch ratio, T/D, was varied from 1.13 to 1.90. Both ends of the cylinders were clamped to the walls of the wind tunnel. Natural frequency and damping ratio of the cylinder model in still air were measured by the method of impulse excitation, thus giving $f_{n0}^* = 69$ Hz and a structural damping ratio $\zeta_s = 0.120$, respectively. The properties of the cylinder model are summarized in Table 1.

In the present experiment, the pitch ratio range investigated is $1.13 \leqslant T/D \leqslant 1.9$. Therefore, the blockage ratio for $T/D = 1.9$ is 10% because the two cylinders are wide enough apart to behave like two separate cylinders. For $T/D = 1.13$, the blockage ratio is ~10.6% because the two cylinders are close enough to behave like a single bluff body. Compared with similar two-cylinder cases studied in the literature, e.g., in the study of Zhou et al. (2001), the blockage is 3.4% and in Xu et al. (2003) the blockage is 13.3%; the present blockage ratio lies within the range of 3.34–13.3%. Furthermore, in the study of So and Savkar (1981) on a single cylinder in a nonturbulent and a turbulent cross-flow, the effect of blockage was investigated and compared to data in the literature (Wieselsberger, 1923; Richter and Naudascher, 1976). The blockage range examined varies from zero to 32%. In their study, the result showed that increasing the blockage ratio does not change the behavior of the mean drag curve versus Re. However, the magnitude of the mean drag increases with increasing Re in the subcritical regime, and the Re at which transition to the critical range takes place is pushed backward as blockage increases. Therefore, it is reasonable to assume that the 10% or so blockage will not affect the characteristics of the biased gap flow and the effect of free-stream turbulence on the biased gap flow could still be discerned with the present experimental set-up.

2.3. Measurement of cylinder vibrations

In the experiment, U_∞ was increased from 3 to 25 m/s, and cylinder displacement at the mid-span of two cylinders was measured using a vibration testing system, for a number of mean velocities when the turbulence generation grid was absent or present. In the system, the vibration signal was picked up by a laser vibrometer (Polytec, Model OFV 3001) and conditioned by a charge amplifier. Afterwards, the signal was sampled by the LabView system and recorded in a personal computer. The measurements are nondimensionalized with respect to U_∞ and D for further analysis.

Preliminary spectral analysis of the measured data showed that there exists an extremely low-frequency component (close to $f = 0$, where f is the dimensionless frequency) at some reduced velocities. This component is due to the direct-current (DC) shift of the laser vibrometer and should be eliminated in order to obtain true information about the amplitude of vibration due to fluid flow. Furthermore, there are some low-frequency components around $f = 0.05$. They could be attributed to the vibration and the end effect of wind tunnel walls (Shirakashi et al., 1985), thus these low-frequency components should also be filtered.

Consequently, a filter based on continuous wavelet transform (CWT) is applied to the measured data to filter out the low-frequency components. In the present preliminary data processing, the CWT-based filter is applied to the measured cylinder displacements with the low frequency bound set at $f_{\text{low}} = 0.0009 \approx 0$ and the high frequency bound set at $f_{\text{up}} \approx 0.05$, i.e., a band-pass filter is actually used with a high cut-off frequency set at around 0.05.

3. Results and discussion

The primary quantity measured in the experiment is the vibration displacement at mid-span of the two cylinders with five pitch ratios, $T/D = 1.17$, 1.30, 1.50, 1.70, and 1.90, for both nonturbulent and turbulent free-stream flow conditions. For each value of T/D, cylinder vibration at 12 different values of reduced velocity, in the range of $U_{r0} = 1.45$–12.08, are studied. The effect of wake interference on the vibration displacement is analyzed first. This is followed by an analysis of the free-stream turbulence effect by comparing with the results of the one-cylinder case. Hereafter, the terminology ''two-cylinder'' and ''one-cylinder'' are used to denote the present and previous (So et al., 2007) experiments. A further energy analysis is carried out to explore how the energy is transmitted from the turbulent flow to cylinder vibration.

3.1. Wake interference effect on flow-induced vibration

The measured data for the case of nonturbulent oncoming flow is analyzed first. The root-mean-square (r.m.s.) values of the mid-span displacements of the two cylinders are calculated as a function of U_{r0}, and the results are shown in Fig. 2. The results for the one-cylinder case, where the cylinder structural properties are identical to those of the two-cylinder case, are also given for comparison.

At each of the five pitch ratios investigated, the two cylinders show similar behavior, as seen from Fig. 2. When $T/D < 1.50$ (Figs. 2(a)–(c)), the vibration level of each cylinder is significantly reduced due to wake interference, as compared to the one-cylinder case. In particular, the abrupt increment of vibration due to the lock-in resonance as in the one-cylinder case is not observed; the cylinder vibration appears to be almost constant in the range of U_{r0} studied. When T/D is increased to 1.70, the vibration level becomes high in the range of large U_{r0} ($U_{r0} > 9.18$). From Fig. 2(d), it can be seen that the r.m.s. value of displacement of Cylinder 1 (the upper one shown in Fig. 1(a)) becomes even higher than that of a single cylinder. When $T/D = 1.90$, the vibration level drops in the range of large U_{r0}, but increases in the range of $5.31 < U_{r0} < 7.25$ (Fig. 2(e)). This is usually the region of lock-in resonance for a single cylinder; hence, it is possible that the behavior begins to approach that of the one-cylinder case at this T/D value. It should be noted that, when the spacing between the two cylinders is large ($T/D > 2.3$), the two cylinders behave like two coupled single cylinders whose vibration displacements are out-of-phase, i.e., the phase difference between them is π. At $T/D = 1.90$, the phase difference between the displacements of the two cylinders is calculated and found to vary with U_{r0} in the range of 0.37π–0.43π. For the other four values of T/D, the phase difference is similar, except that the variation of phase difference is slightly increased to the range of 0.36π–0.48π.

Spectral analysis of cylinder displacement data is carried out using the program provided by the MATLAB signal-processing toolbox, in order to understand the above behavior further. The calculated power spectral density (PSD) functions for all five T/D values are shown in Fig. 3. Each PSD function is normalized so that its integration over the frequency domain gives the square of the r.m.s. value of the displacement. It is found that the two cylinders vibrate at multiple frequencies of vortex shedding in response to the vortex-induced force, and at the fundamental natural

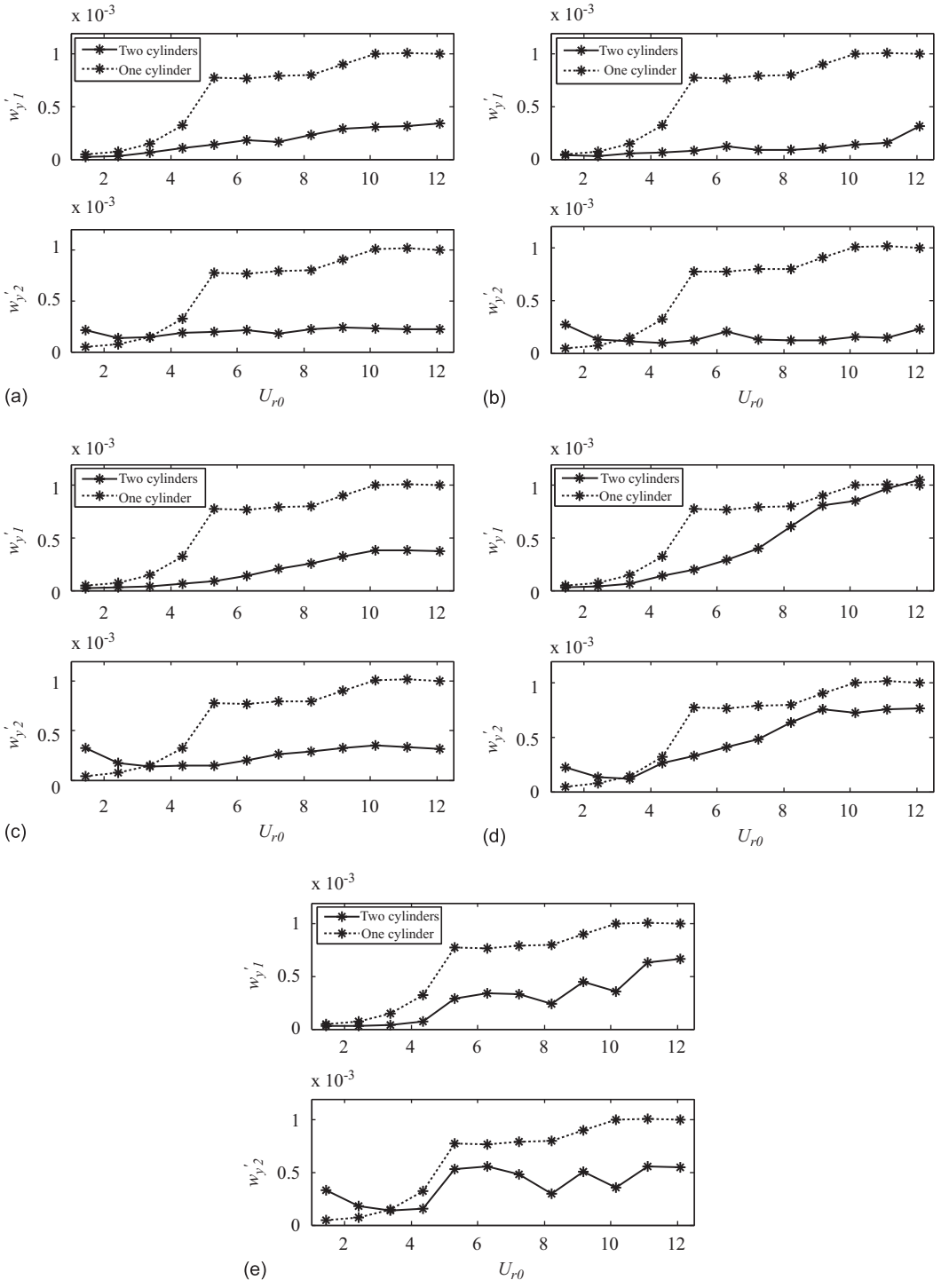

Fig. 2. The root-mean-square values of cylinder displacement for various pitch ratios. (a) $T/D = 1.17$; (b) $T/D = 1.30$; (c) $T/D = 1.50$; (d) $T/D = 1.70$; and (e) $T/D = 1.90$. The subscript in w_y' (the label on the vertical axis of all panels in Fig. 2) denotes cylinder number.

frequency of the cylinder. It should be noted that the natural frequency of the cylinder is affected by the surrounding fluid flow, hence is different from that of a cylinder in still air. It is more appropriate to consider this natural frequency as that of the fluid–cylinder system, denoted by f_n^* in order to differentiate from its counterpart in still air, f_{n0}^*. In dimensionless form, they are represented by $f_n = f_n^* D/U_\infty$ and $f_{n0} = f_{n0}^* D/U_\infty$, respectively. The appearance of cylinder vibration at f_n implies the existence of a negative fluid-damping force, which feeds energy to the cylinder to compensate for energy dissipation due to positive structural damping. As a result, a steady cylinder vibration is maintained at the natural frequency of the fluid–cylinder system, f_n. In the following, the components of cylinder vibration due to the vortex-induced excitation and the fluid-damping force are denoted by w_{yV} and w_{yM}, respectively.

The multiple frequencies of vortex shedding, St, and the natural frequency of the fluid–cylinder system, f_n, are identified from the results of spectral analysis and plotted in Fig. 4 as a function of U_{r0} for all five T/D values. In these figures, the dominant frequencies are marked by solid symbols. For convenience of discussion, the variation of the fundamental natural frequency of the cylinders in still air, f_{n0}, is plotted as a dashed curve, and three straight solid lines corresponding to $f = 0.1$, 0.2, and 0.3 are also shown.

A common feature of the two-cylinder behavior at all five T/D values is that the component w_{yV} is dominant in the low U_{r0} range, where St has a single value in general but decreases with U_{r0} (also Re) from St ≈ 0.3 to ≈ 0.1. There exists a transition value of U_{r0}, at which St becomes multiple-valued and the component w_{yM} becomes significant. This feature is consistent with that of two stationary cylinders (Xu et al., 2003), but appears more complex due to the influence of cylinder vibration. The behavior after the transition is different for different T/D values, and will be discussed individually as follows.

At $T/D = 1.17$, the transition occurs at $U_{r0} = 3.38$ (Re = 11 570), where St changes from a single value around 0.1 to triple values around 0.1, 0.2, and 0.3. At this transition point, w_{yM} becomes as dominant as w_{yV} for Cylinder 1, and more dominant than w_{yV} for Cylinder 2. Afterwards, cylinder vibration is dominated by w_{yM} in general. In the range of $4.35 < U_{r0} < 7.25$, St has double values, one around 0.1 and the other complies with f_n. When U_{r0} increases to the range $9.18 < U_{r0} < 11.11$, the lower St diminishes and the higher St coincides with f_n. However, the induced cylinder vibration is not significant. At $U_{r0} = 12.08$, St ≈ 0.1 and is separated from f_n.

At $T/D = 1.30$, the transition occurs at $U_{r0} = 5.31$ (Re = 18 182) for Cylinder 1 and 4.35 (Re = 14 876) for Cylinder 2, where St changes from a single value around 0.1 to double values around 0.1 and 0.3. Different from the case of $T/D = 1.17$, w_{yV} is dominant after the transition in the range of $5.31 < U_{r0} < 6.28$, at St ≈ 0.3. Afterwards, both w_{yV} and w_{yM} are dominant in the range of $7.25 < U_{r0} < 9.18$, then w_{yV} becomes dominant again in the range of $10.15 < U_{r0} < 12.08$. This implies that the contribution of w_{yM} is not as significant as for $T/D = 1.17$. The behavior at $T/D = 1.50$ is similar to that at $T/D = 1.30$, except that St and f_n are very close to each other in the range of $7.25 < U_{r0} < 9.18$. This might explain why the amplitude of cylinder vibration has an increment in this range, as compared with the case of $T/D = 1.30$.

When the pitch ratio is increased to $T/D = 1.70$, the transition occurs at $U_{r0} = 3.38$, where St changes from a single value around 0.2 to double values around 0.1 and 0.3. Afterwards, the behavior appears to be similar to that at $T/D = 1.50$. However, a careful inspection shows that the frequency of cylinder vibration at $T/D = 1.70$ is closer to the curve of f_{n0}, particularly in the range of $9.18 < U_{r0} < 12.08$. This suggests that cylinder vibration is more relevant to the fluid damping force.

At $T/D = 1.90$, the transition occurs earlier, at $U_{r0} = 2.42$, where a single St value around 0.2 changes to double values around 0.2 and 0.3, then further develops to triple values around 0.1, 0.2, and 0.3 at $U_{r0} = 3.38$, and it changes back to double values around 0.1 and 0.3 at $U_{r0} = 4.35$. In the range of $2.42 < U_{r0} < 4.35$, vibration associated with the lower St dominates in Cylinder 1, while that with the higher St dominates in Cylinder 2. This is a typical response of the cylinders to the excitation arising from biased gap flow. At $U_{r0} = 5.31$, vibrations of both cylinders become dominated by the higher St around 0.3, where St and f_n coincide and vibration level becomes high. The coincidence happens again at $U_{r0} = 8.21$ and 9.18, where St shifts to around 0.2, giving rise to another region of high-level vibration. In the range of $10.15 < U_{r0} < 12.08$, w_{yM} becomes dominant.

3.2. Turbulence effect on flow-induced vibration

The same procedure of data analysis is applied to the measured data for the case of turbulent approach flow to study free-stream turbulence effect on flow-induced vibration. The r.m.s. values of the mid-span displacements of the two cylinders are calculated as function of U_{r0}, and the results are displayed in Fig. 5.

For the one-cylinder case, it has been shown that the effect of free-stream turbulence is to promote w_{yV} in the lock-in resonance region and w_{yM} in the region of large U_{r0} (So et al., 2007). For the present two-cylinder case, the values of U_{r0} at which the enhancement is significant are identified from Fig. 5 and listed in Table 2. It can be seen that free-stream

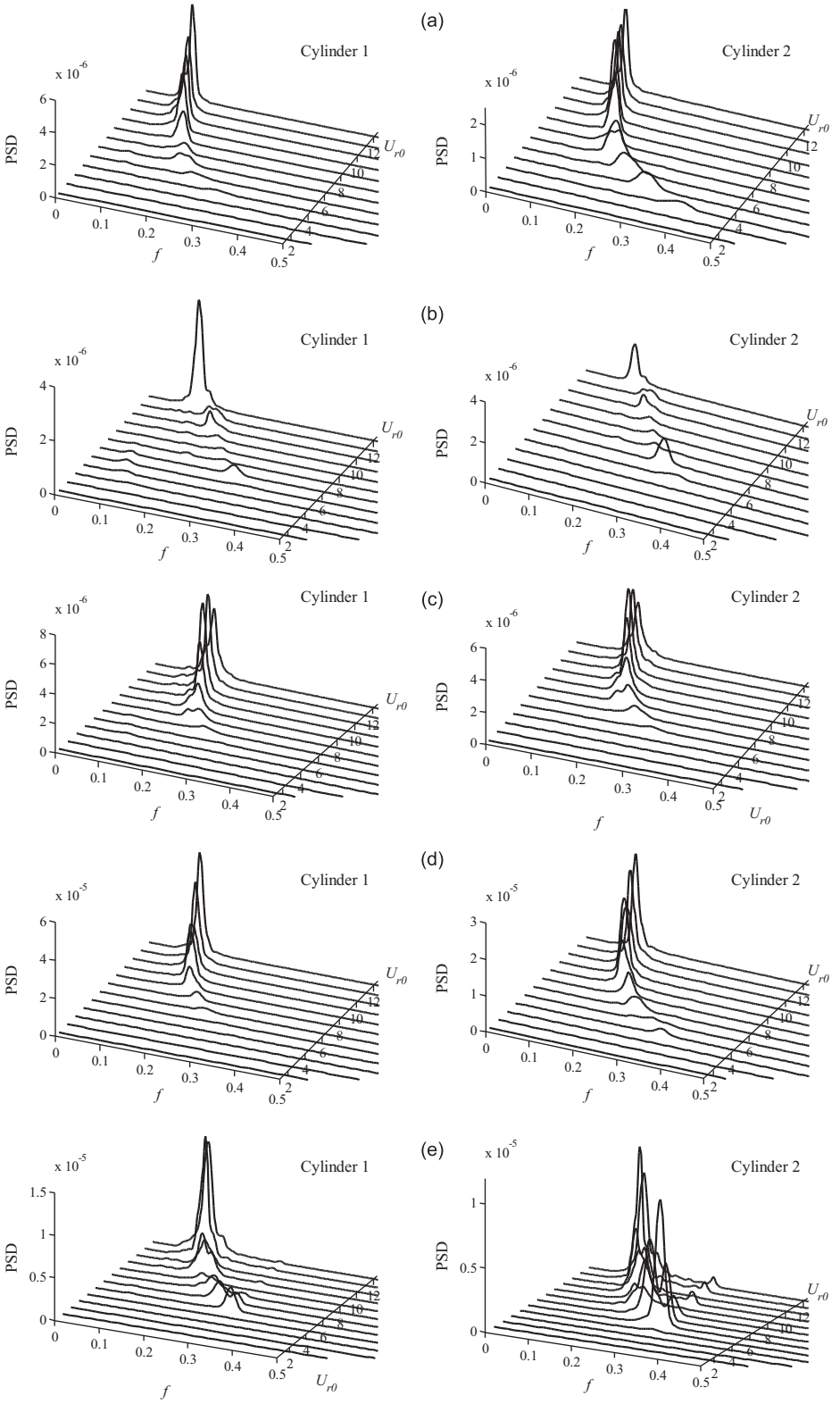

Fig. 3. Plots of power spectral density (PSD) function of cylinder displacement for the case of nonturbulent approach flow. (a) $T/D = 1.17$; (b) $T/D = 1.30$; (c) $T/D = 1.50$; (d) $T/D = 1.70$; and (e) $T/D = 1.90$.

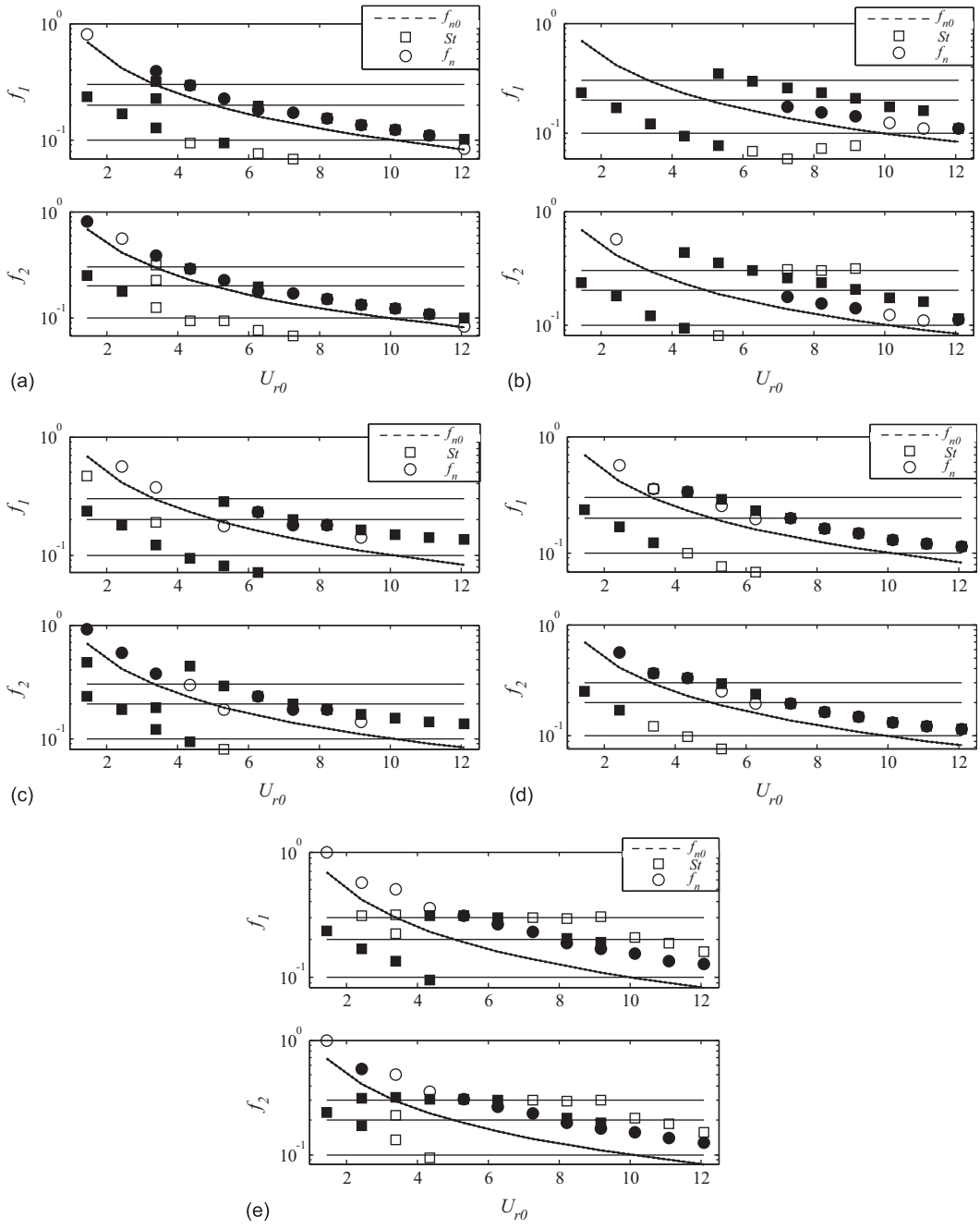

Fig. 4. Dominant frequencies of cylinder displacement for the case of nonturbulent approach flow. (a) $T/D = 1.17$; (b) $T/D = 1.30$; (c) $T/D = 1.50$; (d) $T/D = 1.70$; and (e) $T/D = 1.90$.

turbulence still enhances cylinder vibration, but at different U_{r0} values for different T/D. This will be discussed in detail along with the results of spectral analysis in the following.

The results of spectral analysis of cylinder displacement data are plotted in Fig. 6. Each PSD function is normalized so that its integration along the frequency domain gives the square of the r.m.s. value. Same as the case of nonturbulent approach flow, the two cylinders vibrate at multiple frequencies of vortex shedding in response to the vortex-induced force, and at the fundamental natural frequency of the fluid–cylinder system due to the fluid-damping force.

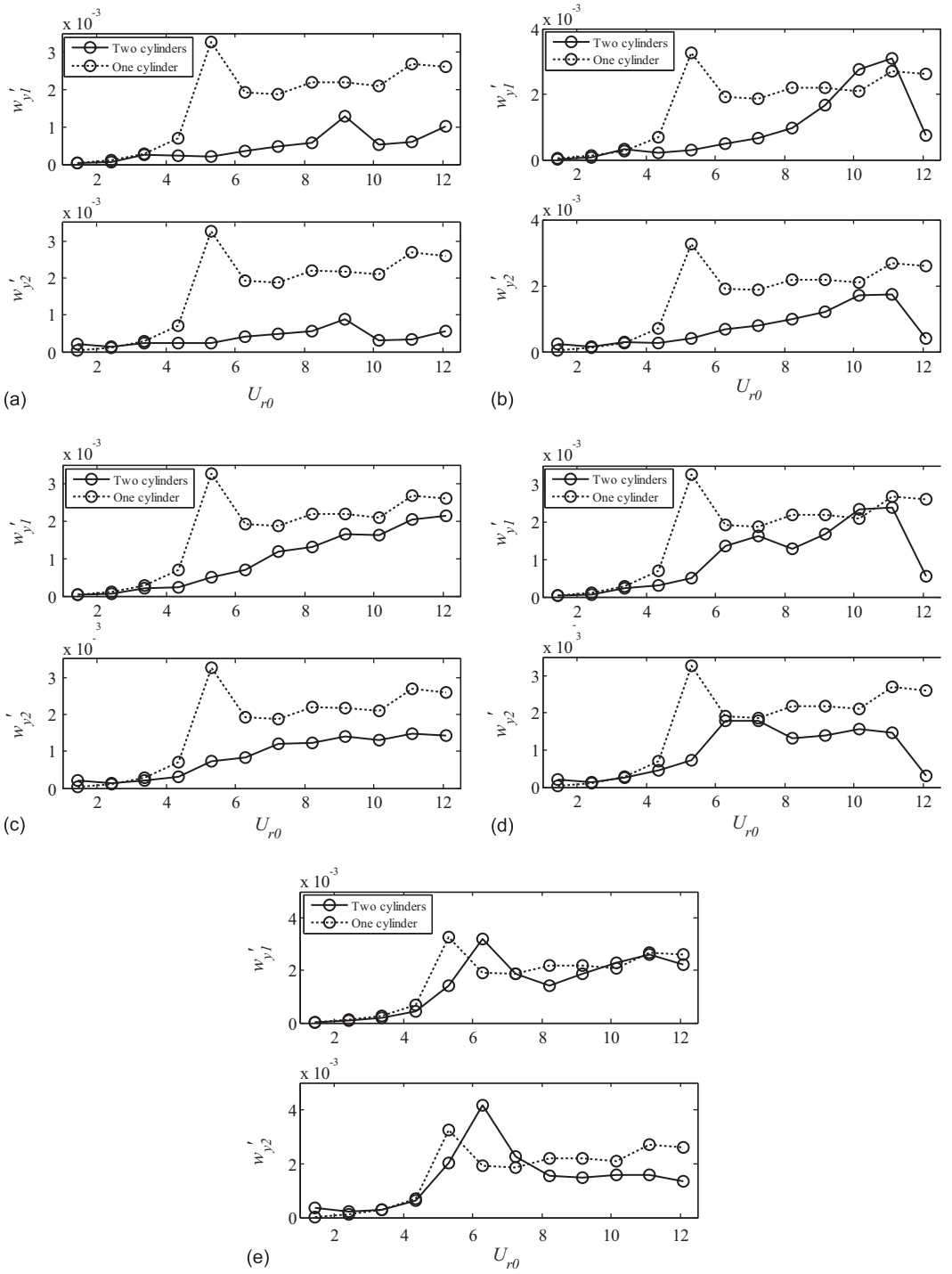

Fig. 5. The root-mean-square values of cylinder displacement for the case of turbulent approach flow. (a) $T/D = 1.17$; (b) $T/D = 1.30$; (c) $T/D = 1.50$; (d) $T/D = 1.70$; and (e) $T/D = 1.90$.

Variations of these frequencies with U_{r0} are plotted in Fig. 7 for all five T/D values, where the dominant frequencies are marked by solid symbols. Again, the variation of f_{n0} is plotted as a dashed curve. In addition, three straight solid lines, corresponding to $f = 0.1$, 0.2, and 0.3, respectively, are also shown.

Table 2
Values of U_{r0} at which the enhancement of cylinder vibration due to free-stream turbulence is significant

T/D	U_{r0}	$f_0 = 1/U_{r0}$
1.17	9.18	0.11
1.30	11.11	0.09
1.50	12.08	0.08
1.70	7.25, 10.15	0.14, 0.10
1.90	6.28	0.16

At $T/D = 1.17$ and 1.30, free-stream turbulence promotes cylinder vibration at $U_{r0} = 9.18$ and 11.11, corresponding to $f_0 = 0.11$ and 0.09, respectively. At $T/D = 1.17$, the peak amplitude of cylinder vibration is only about $\frac{1}{3}$ or less of that in the one-cylinder case. At $T/D = 1.30$, the peak amplitude of cylinder vibration is higher and is in the same level as that in the one-cylinder case.

The results of spectral analysis are similar for $T/D = 1.17$ and 1.30, as seen from Figs. 7(a) and (b). In the low U_{r0} range, w_{yV} is dominant, and St is of single value, varying from 0.3 to 0.1 when U_{r0} increases from 1.45 to 3.38. At $U_{r0} = 4.35$, St undergoes a transition from single-value around 0.1 to double-value around 0.1 and 0.3. The cylinder vibration is dominated by w_{yV} until $U_{r0} = 5.31$. However, St changes to a single value around 0.2. Afterwards, the contribution of w_{yM} begins to increase so that both w_{yV} and w_{yM} are dominant in the range of $6.28 < U_{r0} < 8.21$. When U_{r0} increases further, St and f_n coincide, resulting in the resonance peak at $U_{r0} = 9.18$ for $T/D = 1.17$ and at $U_{r0} = 11.11$ for $T/D = 1.30$. This suggests that the two cylinders behave like a single bluff body with $\mathrm{St} \approx 0.1$ when the pitch ratio is small. As a result, cylinder vibration due to vortex-induced lock-in resonance is significant, and would be an issue to be considered for two side-by-side cylinders in a turbulent flow environment.

At $T/D = 1.50$, the vibration amplitude of Cylinder 1 increases with U_{r0} and reaches a maximum value at $U_{r0} = 12.08$, which corresponds to $f_0 = 0.08$, while that of Cylinder 2 increases with U_{r0} and reaches a maximum value as early as at $U_{r0} = 9.18$ ($f_0 = 0.11$), then it becomes almost constant.

At $T/D = 1.50$, the results are different from the cases of $T/D = 1.17$ and 1.30; the enhancement of w_{yV} is not very significant, as seen from the results of spectral analysis shown in Fig. 7(c). The behavior of the PSD functions in the low U_{r0} range is similar to that for $T/D = 1.17$ and 1.30. In the range of $5.31 < U_{r0} < 8.21$, however, St and f_n appear to be closer to each other, and both w_{yV} and w_{yM} are dominant. This could explain the increment of vibration level in this range. Afterwards, w_{yM} becomes dominant in cylinder vibration in the range of $9.18 < U_{r0} < 12.08$. Overall, the enhancement is at the natural frequency of the fluid–cylinder system rather than at the frequencies of vortex shedding.

At $T/D = 1.70$, two resonance peaks are observed at $U_{r0} = 7.25$ and 10.15, corresponding to $f_0 = 0.14$ and 0.10, respectively; the former being more pronounced for Cylinder 1 while the latter more pronounced for Cylinder 2. This could be attributed to the complex situation of vortex shedding, as seen from the results of spectral analysis shown in Fig. 7(d). It can be seen that St and f_n coincide in two ranges, one in $5.31 < U_{r0} < 6.28$ and another in $9.18 < U_{r0} < 12.08$, giving rise to large vibration amplitudes. In between, at $U_{r0} = 8.21$, w_{yM} is dominant but w_{yV} is present also, and St takes on triple values. This implies that free-stream turbulence promotes vortex-induced vibration at two Strouhal numbers for the two cylinders with this T/D value.

At $T/D = 1.90$, the behavior of the two cylinders is similar to that of a single cylinder, except that the vibration peak occurs at $U_{r0} = 6.28$, which corresponds to $f_0 = 0.16$. Moreover, the maximum amplitude of vibration of Cylinder 1 is approximately identical to that of a single cylinder, while that of Cylinder 2 is larger by about $\frac{1}{3}$. For this T/D value, the results of spectral analysis are shown in Fig. 7(e). It can be seen that the range where St and f_n coincide is shifted to $4.35 < U_{r0} < 6.28$. In the low U_{r0} range, w_{yV} is dominant while St is essentially around 0.2. In the large U_{r0} range, w_{yM} becomes dominant, while St is still around 0.2. Therefore, the behavior is very similar to that of the one-cylinder case.

3.3. Turbulence effect from the energy point of view

When turbulent fluctuations are present in the mean flow, energy imparted to the fluid–cylinder system is increased if the mean flow velocity remains unchanged. In general, whether the energy is transmitted to the cylinder or extracted from the cylinder, and how much this energy transmission might be, depends on the nature of cylinder vibration. This can be demonstrated by comparing the energies of the cylinder for the nonturbulent and turbulent flow cases. The energies of the cylinders can be studied by examining the ratio of increment of displacement squared, which can be

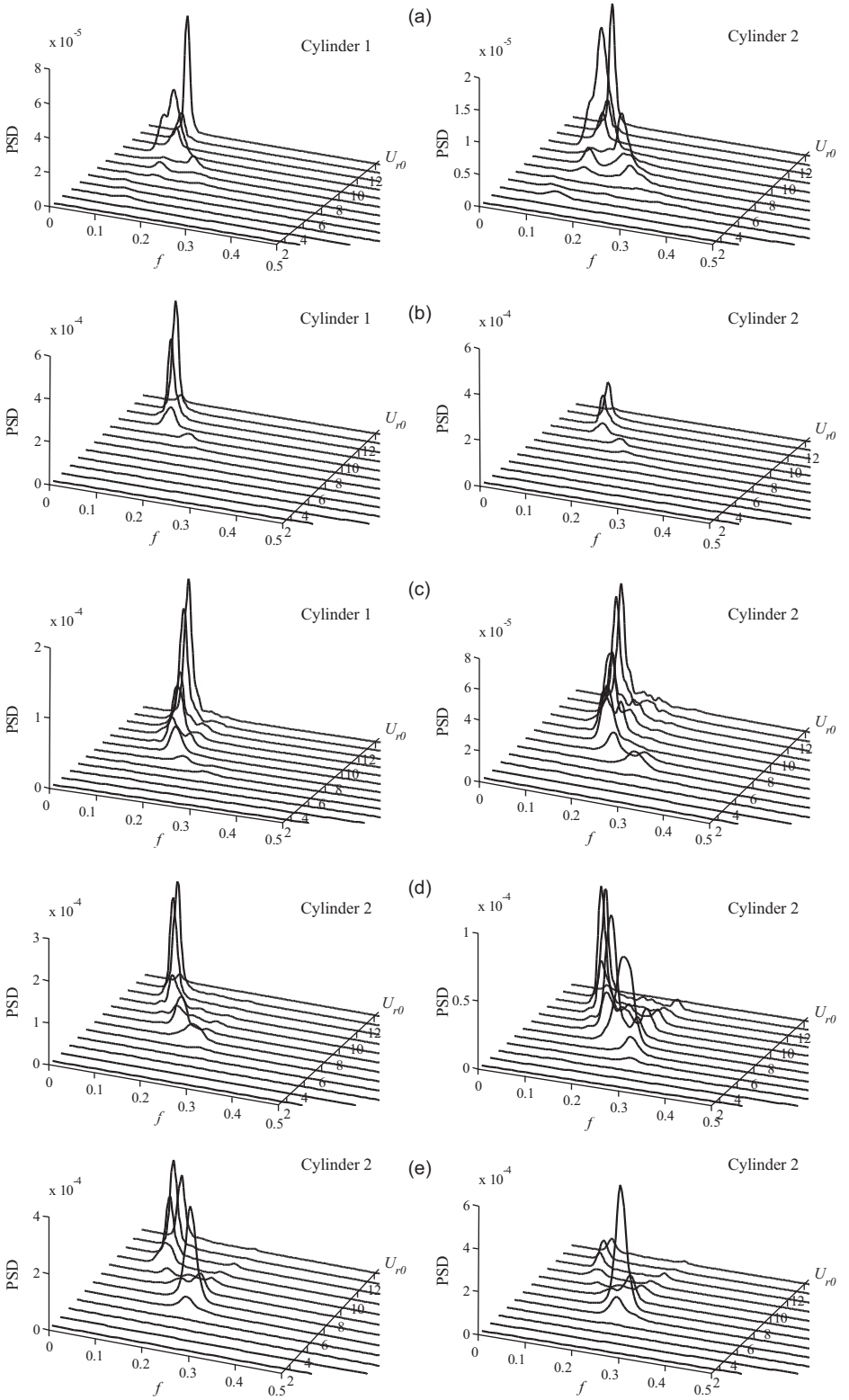

Fig. 6. Plots of power spectral density (PSD) function of cylinder displacement for the case of turbulent approach flow. (a) $T/D = 1.17$; (b) $T/D = 1.30$; (c) $T/D = 1.50$; (d) $T/D = 1.70$; and (e) $T/D = 1.90$.

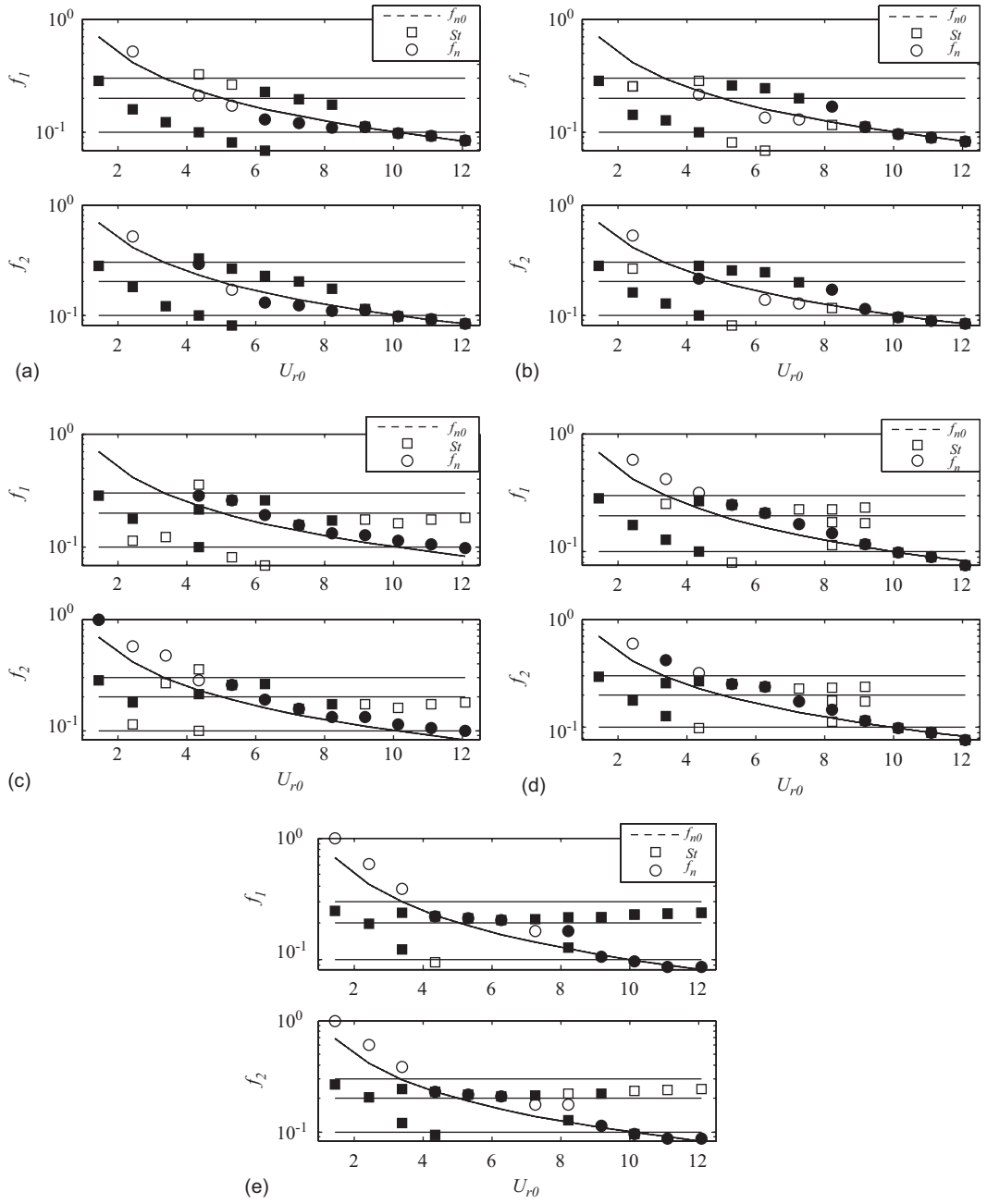

Fig. 7. Dominant frequencies of cylinder displacement for the case of turbulent approach flow. (a) $T/D = 1.17$; (b) $T/D = 1.30$; (c) $T/D = 1.50$; (d) $T/D = 1.70$; and (e) $T/D = 1.90$.

defined as

$$r_{wi} = \frac{w_{ti}'^2 - w_{ui}'^2}{w_{ui}'^2}, \quad i = 1, 2,$$

where w_{ui}' and w_{ti}' are r.m.s. values of the displacement for nonturbulent and turbulent flow, respectively; the subscript numbers $i = 1$ and 2 represent the upper and the lower cylinders (Fig. 1(a)), respectively. The displacement squared is

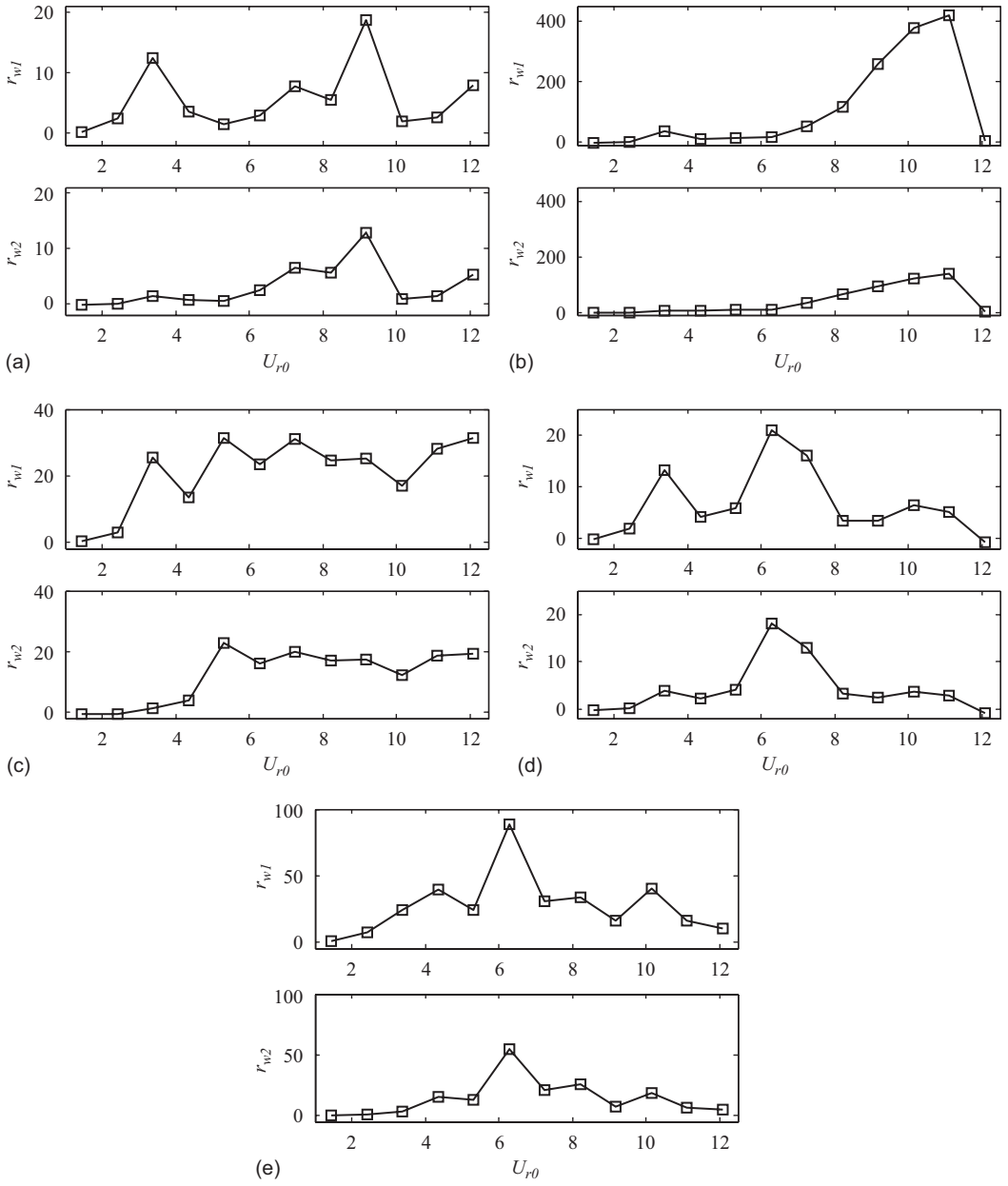

Fig. 8. Ratio of energy increment of the two cylinders due to free-stream turbulence. (a) $T/D = 1.17$; (b) $T/D = 1.30$; (c) $T/D = 1.50$; (d) $T/D = 1.70$; and (e) $T/D = 1.90$.

an indicator of kinetic energy for the two cylinders, and its behavior is consistent with that of the total energy (So et al., 2007).

For all five T/D values, the results of r_{wi} are plotted against U_{r0} in Fig. 8. It can be seen that the ratio has a peak within the lock-in region whenever lock-in resonance occurs. This suggests that the main effect of free-stream turbulence is to enhance vortex shedding. The enhancement reaches its maximum at $T/D = 1.30$, where the peak value is as high as 400. This is possibly because $\mathrm{St} \approx 0.09$ ($U_{r0} = 11.11$) at this pitch ratio, which is easier to be excited. At $T/D = 1.17$, one more peak is observed at $U_{r0} = 3.38$ ($\mathrm{St} \approx 0.3$). This means that energy is fed to the cylinders at two Strouhal numbers. At $T/D = 1.50$, no peak is observed; r_{wi} appears to have a sudden jump at $U_{r0} = 5.31$, and keeps almost constant afterwards. This suggests that energy is fed to the cylinders not only by promoting vortex shedding but

also enhances the motion-dependent excitation. At $T/D = 1.70$, three peaks can be identified at $U_{r0} = 3.38$, 6.28, and 10.15, implying three Strouhal numbers arising from wake interference, at $St = 0.30$, 0.16, and 0.10, respectively. At $T/D = 1.90$, there are still three peaks, but one of them changes from $U_{r0} = 3.38$ to 4.35.

4. Conclusions

The effect of free-stream turbulence on vortex-induced vibration of two side-by-side elastic cylinders in a cross-flow was investigated experimentally. The experiments were carried out in a wind tunnel with the ends of the elastic cylinders fixed just outside the walls of the wind tunnel. Five pitch ratios in the regime of biased gap flow were considered, i.e., $T/D = 1.17$, 1.30, 1.50, 1.70, and 1.90. A turbulence generation grid was installed to create a flow with a turbulence intensity around 10%.

Cylinder vibration in the transverse direction was measured at the mid-span of the two cylinders. For uniform approach flow, vortex-induced vibration is reduced due to wake interference when $T/D < 1.50$. At $T/D = 1.70$, cylinder vibration becomes large in the large U_{r0} range, compatible to that of a single cylinder. When T/D is increased further, the behavior becomes similar to that of a single cylinder, but the vibration level is not as high. The behavior of the two cylinders shows a slight difference due to the influence of biased gap flow. Spectral analysis of the vibration data showed that there are two dominant components: one occurring at multiple frequencies of vortex shedding and the other at the fundamental natural frequency of the fluid–cylinder system. These displacement components are denoted by w_{yV} and w_{yM}, respectively. While w_{yV} is due to the vortex-induced force, w_{yM} is considered to be maintained by the fluid-damping force. Although the fluid–structure system natural frequency coincides with the frequencies of vortex shedding at several values of U_{r0}, cylinder vibration associated with the lock-in resonance is not as significant as for the one-cylinder case.

In general, the effect of free-stream turbulence is to enhance vortex shedding, thus restoring the large-amplitude vibration associated with lock-in resonance. The enhancement is at different Strouhal numbers for different pitch ratios. When the spacing between two cylinders is relatively small ($1.17 < T/D < 1.50$), the enhancement is significant at $St \approx 0.1$, suggesting that the two cylinders behave like a single bluff body. The value of $T/D = 1.50$ appears to be a transition point, at which the enhancement is more significant at the natural frequency of the fluid–cylinder system. At this value, the biased gap flow appears to affect the fluid-damping force in the range of large U_{r0} values, and the influence is slightly different for the two cylinders. When the pitch ratio exceeds this value, the Strouhal number at which the enhancement is significant tends to shift from $St \approx 0.1$ to ≈ 0.16 (at $T/D = 1.90$). In the shifting process, the enhancement may occur at multiple Strouhal numbers ($T/D = 1.70$).

An energy analysis showed that free-stream turbulence feeds energy to the cylinder at multiple frequencies of vortex shedding. Therefore, the lock-in region is still of main concern when the approach flow is turbulent, as in the case of a single elastic cylinder in a cross-flow. For the present case of two side-by-side cylinders, however, the lock-in resonance occurs at a different Strouhal number, depending on the pitch ratio. Therefore, the range of U_{r0} to be concerned is broadened.

Acknowledgment

Funding support from the Research Grants Council of the Government of the HKSAR under Projects PolyU5307/03E and PolyU5321/04E are gratefully acknowledged.

References

Alam, M.M., Moriya, M., Sakamoto, H., 2003. Aerodynamic characteristics of two side-by-side circular cylinders and application of wavelet analysis on the switching phenomenon. Journal of Fluids and Structures 18, 325–346.

Bearman, P.W., Wadcock, A., 1973. The interaction between a pair of circular beams normal to a stream. Journal of Fluid Mechanics 61, 499–511.

Chang, K.-S., Song, C.-J., 1990. Interactive vortex shedding from a pair of circular cylinders in a transverse arrangement. International Journal for Numerical Methods in Fluids 11, 317–329.

Chen, S.S., 1986. A review of flow-induced vibration of two circular beams in crossflow. ASME Journal of Pressure Vessel Technology 108, 382–393.

Chen, L., Tu, J.Y., Yeoh, G.H., 2003. Numerical simulation of turbulent wake flows behind two side-by-side cylinders. Journal of Fluids and Structures 18, 387–403.

Guillaume, D.W., LaRue, J.C., 1999. Investigation of the flopping regime with two-, three-, and four-cylinder arrays. Experiments in Fluids 27, 145–156.

Guillaume, D.W., LaRue, J.C., 2003. Investigation of peak frequencies in the flopping regime with a two-cylinder array. Journal of Fluids and Structures 17, 331–335.

Ichioka, T., Kawata, Y., Nakamura, T., Izumi, H., Kobayashi, T., Takamatsu, H., 1997. Research on fluid elastic vibration of beam arrays by computational fluid dynamics (analysis of two beams and a beam row). JSME International Journal Series B 40, 16–24.

Jester, W., Kallinderis, Y., 2003. Numerical study of incompressible flow about fixed cylinder pairs. Journal of Fluids and Structures 17, 561–577.

Kim, H.J., Durbin, P.A., 1988. Investigation of the flow between a pair of circular beams in the flopping regime. Journal of Fluid Mechanics 196, 431–448.

Meneghini, J.R., Saltara, F., Siqueira, C.L.R., Ferrari Jr., J.A., 2001. Numerical simulation of flow interference between two circular cylinders in tandem and side-by-side arrangements. Journal of Fluids and Structures 15, 327–350.

Naudascher, E., Rockwell, D., 1994. Flow-Induced Vibrations: An Engineering Guide. Balkema, Dordrecht.

Ng, C.W., Cheng, V.S.Y., Ko, N.W.M., 1997. Numerical study of vortex interactions behind two circular beams in bistable flow regime. Fluid Dynamics Research 19, 379–409.

Peschard, I., Le Gal, P., 1996. Coupled wakes of cylinders. Physical Review Letters 77, 3122–3125.

Richter, A., Naudascher, E., 1976. Fluctuating forces on a rigid circular cylinder in a confined flow. Journal of Fluid Mechanics 78, 561–576.

Shirakashi, M., Ishida, Y., Wakiya, S., 1985. Higher velocity resonance of circular cylinder in crossflow. ASME Journal of Fluids Engineering 107, 392–396.

Slaouti, A., Stansby, P.K., 1992. Flow around two circular beams by the random-vortex method. Journal of Fluids and Structures 6, 641–670.

So, R.M.C., Savkar, S.D., 1981. Buffeting forces on rigid circular cylinders in cross flows. Journal of Fluid Mechanics 105, 397–425.

So, R.M.C., Wang, X.Q., 2003. Vortex-induced vibrations of two side-by-side Euler–Bernoulli beams. Journal of Sound and Vibration 259, 677–700.

So, R.M.C., Wang, X.Q., Xie, W.-C., Zhu, J., 2007. Free stream turbulence effects on vortex-induced vibration of an elastic cylinder. Journal of Fluids and Structures, accepted for publication.

Sumner, D., Price, S.J., Paidoussis, M.P., 1997. Investigation of impulsively-started flow around two side-by-side circular cylinders: application of particle image velocimetry. Journal of Fluids and Structures 11, 597–615.

Sumner, D., Price, S.J., Paidoussis, M.P., 1999. Fluid behavior of side-by-side circular cylinders in steady cross-flow. Journal of Fluids and Structures 13, 309–338.

Wang, X.Q., So, R.M.C., Xie, W.-C., 2007. Features of flow-induced forces deduced from wavelet analysis. Journal of Fluids and Structures 23, 249–268.

Wieselsberger, G., 1923. Der Widerstand von Zylinder. Ergebnisse der Aerodynamischen Versuchsanstalt Göttingen, II. Lieferung, p. 23.

Williamson, C.H.K., 1985. Evolution of a single wake behind a pair of bluff bodies. Journal of Fluid Mechanics 159, 1–18.

Wradlaw, R.L., 1994. Interference and proximity effects. In: Sockel, H. (Ed.), Wind-Excited Vibrations of Structures. Springer, Berlin.

Xu, S.J., Zhou, Y., So, R.M.C., 2003. Reynolds number effects on the flow structure behind two side-by-side cylinders. Physics of Fluids 15, 1214–1219.

Zdravkovich, M.M., 1997. Flow Around Circular Cylinders, vol. 1. Oxford University Press, Oxford.

Zdravkovich, M.M., 2003. Flow Around Circular Cylinders, vol. 2. Oxford University Press, Oxford.

Zhou, Y., Wang, Z.J., So, R.M.C., Xu, S.J., Jin, W., 2001. Free vibration of two side-by-side cylinders in a cross flow. Journal of Fluid Mechanics 443, 197–229.